Nonlinear simulation of multiple toroidal Alfvén eigenmodes in tokamak plasmas*

Xiao-Long Zhu(朱霄龙), Feng Wang(王丰)†, and Zheng-Xiong Wang(王正汹)‡

Key Laboratory of Materials Modification by Laser, Ion and Electron Beams of the Ministry of Education, School of Physics, Dalian University of Technology, Dalian 116024, *China*

(Received 18 November 2019; revised manuscript received 9 December 2019; accepted manuscript online 12 December 2019)

Nonlinear evolution of multiple toroidal Alfvén eigenmodes (TAEs) driven by fast ions is self-consistently investigated by kinetic simulations in toroidal plasmas. To clearly identify the effect of nonlinear coupling on the beam ion loss, simulations over single-n modes are also carried out and compared with those over multiple-n modes, and the wave-particle resonance and particle trajectory of lost ions in phase space are analyzed in detail. It is found that in the multiple-n case, the resonance overlap occurs so that the fast ion loss level is rather higher than the sum loss level that represents the summation of loss over all single-n modes in the single-n case. Moreover, increasing fast ion beta $\beta_{\rm h}$ can not only significantly increase the loss level in the multiple-n case but also significantly increase the loss level increment between the single-n and multiple-n cases. For example, the loss level in the multiple-n case for $\beta_{\rm h} = 6.0\%$ can even reach 13% of the beam ions and is 44% higher than the sum loss level calculated from all individual single-n modes in the single-n case. On the other hand, when the closely spaced resonance overlap occurs in the multiple-n case, the release of mode energy is increased so that the widely spaced resonances can also take place. In addition, phase space characterization is obtained in both single-n and multiple-n cases.

Keywords: tokamak, toroidal Alfvén eigenmode, wave-particle interaction, beam ion loss

PACS: 52.55.Fa, 52.35.Bj, 94.20.wj, 52.55.Dy **DOI:** 10.1088/1674-1056/ab610e

1. Introduction

Alfvén instability, as a type of magnetohydrodynamic (MHD) instabilities, is very common in both space and laboratory plasmas.[1–3] In present-day fusion and future burning plasmas, Alfvén instability is easily driven to be unstable by the wave-particle interaction, including alpha particles from fusion and fast ions produced by neutral beam injection and other auxiliary heating methods. It can not only affect the plasma confinement and transport but also induce excessive fast ion loss and redistribution. On the other hand, the successful realization of the magnetically confined fusion depends on the satisfactory confinement of the fast ions. In fact, if the fast ion losses are sufficiently localized and intense, they could bring about an unplanned heat load and damage to the first wall, leading to the termination of discharges in tokamaks. Ideally, fast ions and fusion products could be well confined until their energy is transferred to the bulk plasmas. Fully understanding the wave–particle interaction between Alfvén waves and fast ions, the mechanism of fast ion loss, and then developing some methods to control fast ion loss, therefore, are of critical importance for design of plasma-facing materials and reliable predication[4] for the International Thermonuclear Experimental Reactor (ITER) and the China Fusion Engineering Test Reactor (CFETR).[5]

A well-known discrete Alfvén mode is toroidicity-induced Alfvén eigenmode (TAE). The resonant interaction between fast ions and TAE, especially multiple toroidal harmonic mode (multiple-n) TAE, is believed to represent one of the main mechanisms for fast ion loss in ITER.[6] Also, there have been extensive experimental and theoretical investigations on the fast ion losses induced by TAE, including single toroidal harmonic mode (single-n) and multiple-n TAEs, in present-day tokamaks and helical devices. It was observed that a single TAE with fluctuation amplitude above a certain threshold can induce diffusive fast ion loss, and an overlapping of TAE and Alfvén cascades of spatial structures leads to a large fast ion diffusion and loss.[7] The experimental results on the NSTX device showed that up to 40% of the fast-ion population can be expelled from confined plasmas after a TAE avalanche, thus the cumulative effect of a repetitive cycle of avalanches on the plasmas performance is dramatic.[8] In JET advanced tokamak scenario, the core-localized TAE was observed to have a significant impact both on internal redistribution and on the loss of fast ions.[9] Strong TAE activity can induce up to 70% of the fast ion loss.[10] On the DIII-D tokamak, multiple simultaneous small-amplitude Alfvén eigenmodes (AEs) can result in overlapping wave-particle resonances, leading

*Project supported by the National Key R&D Program of China (Grant No. 2017YFE0301900), the National Natural Science Foundation of China (Grant No. 11675083), and the Fundamental Research Funds for the Central Universities of China (Grant No. DUT18ZD101).

†Corresponding author. E-mail: fengwang@dlut.edu.cn

‡Corresponding author. E-mail: zxwang@dlut.edu.cn

to a critical gradient transport phenomenon.[11,12] The critical energetic particle density gradient in an AE stiff transport model has been verified against nonlinear GYRO simulations for a representative DIII-D discharge, and a simple and computationally inexpensive way to estimate the time-averaged steady-state energetic-particle (EP) density in a system with AE-induced EP transport was put forward by Bass and Waltz.[13] It should be noted that the simulation by Bass and Waltz was a local nonlinear simulation. We perform the global and self-consistent nonlinear simulations and assess the TAE-induced EP transport level self-consistently. In addition, HAGIS-LIGKA simulations by Schneller *et al.* showed that the global nonlinear effects are crucial for evolution of the multi-mode scenario, which not only grow amplitudes of multiple modes to higher values compared to the single mode case but also trigger strong redistribution.[14] Furthermore, Chen *et al.* theoretically showed that in future the presence of negative neutral beam injection induced energetic particle tail will make the system more unstable and prone to losses.[15] These results present a fairly complex pattern, only part of which is understood at present. Fast ions can be lost through various processes, such as prompt loss,[16] non-resonant loss,[16] mode-particle pumping,[17] and ripple loss.[18] Prompt losses are losses of particles born on perturbed orbits that collide with the first wall before they finish one or several poloidal transits, which may result from local wave particle resonant interaction.[16,19] The non-resonant ions can exchange energy with the wave, but the net contributed energy may be nearly zero, as the energy gained during one phase of wave is lost during the next opposite phase for these confined non-resonant ions. However, when a loss boundary exists, the case can vary. If an ion interacts with the wave for less than a full circle, the net contributed energy will not be negligible. Mode-particle pumping is a resonance phenomenon, which is an interaction of large-scale (global) MHD modes with the particle drift motion over many mode periods.[17] Accordingly, understanding the underlying physics of loss induced by single-n and multiple-n TAEs, especially in the loss mechanism and phase-space characterization, is still rare and badly needed.

In this work, taking into account the beam ion distribution function with the pitch angle scattering, we study the nonlinear evolution of multiple TAEs by means of kinetic simulations with the M3D-K code. Two kinds of cases are performed: one is the single-n TAE case, the other is the multiple-n case. The focus is on the understanding of the principle physics behind the loss induced by single-n and multiple-n TAEs and the phase-space characterization of losses. The wave-particle resonance and particle trajectory of lost ions in phase space in both the cases are obtained and compared. It is found that the fast ion loss level induced by the relatively strong resonance-overlapping multiple-n TAE is greatly enhanced. Finally, we also compare the percentages of different lost particles in different cases.

The remainder of this paper is organized as follows: Section 2 briefly describes the global nonlinear kinetic-MHD hybrid simulation code M3D-K used in this work. The main parameters and equilibrium, the simulation results including the single-n TAE and the multiple-n TAE are discussed and analyzed in Section 3. Finally discussions and conclusions are given in Section 4.

2. Equilibrium profiles and parameter setup

This work is performed by using the global nonlinear kinetic-MHD hybrid initial value code M3D-K for toroidal plasmas.[20,21] In the code, the plasmas consist of two components: the thermal component and the energetic component. The thermal component including thermal ions and electrons is described as a single fluid by resistive MHD equations solved via the finite element method. The energetic component is treated by drift-kinetic equations calculated via the δf particle-in-cell method. The energetic particle effect enters our model through coupling the energetic particle pressure tensor $P_{\rm h}$ to the momentum equation. The M3D-K code has been widely used to investigate the non-resonant kink mode,[22] nonlinear dynamics of fishbone mode,[23–25] TAE,[26,27] EPM,[28–30] and effects of energetic particles on tearing mode.[31]

In the simulation, the chosen safety factor q is $q = 1.1 + \psi$, where ψ is the normalized poloidal magnetic flux in code units varying from 0 at the magnetic axis to 1 at the edge. The main parameters are as follows: circular cross section $R_0/a = 3.11$, Alfvén speed $\upsilon_{\rm A}$, Alfvén time $\tau_{\rm A} = R/\upsilon_{\rm A}$, the central beta of both thermal plasma and energetic particle $\beta_{\rm total,0} = 3.43\%$, and the fraction of energetic particles $\beta_{\rm beam} = 1.81\%$.

The injection speed of beam ions is $\upsilon_{\rm h} = 2.55\upsilon_{\rm A}$ in the simulation. The fast ion distribution is slowing down in energy, peaked in pitch angle parameter ($\Lambda = \mu B_0/E$), where μ is the magnetic moment. The form is given by

$$\begin{aligned} f_0 = {} & \frac{c}{(\upsilon^3+\upsilon_{\rm c}^3)}\exp\left[\left(-\frac{P_\phi - \langle \upsilon_\parallel I/\Omega_{\rm h}\rangle}{\Delta\psi}\right)\right] \\ & \times\left(1+{\rm erf}\left(\frac{1-\Lambda_0}{\Delta\Lambda}\right)\right)\times\frac{1}{\Delta\Lambda} \\ & \times\left({\rm erf}\left(\frac{1-\Lambda_0}{\Delta\Lambda}\right)+{\rm erf}\left(\frac{\Lambda_0}{\Delta\Lambda}\right)\right)\exp\left[-\frac{(\Lambda-\Lambda_0)^2}{\Delta\Lambda}\right], \end{aligned} \tag{1}$$

where

$$\Delta\Lambda = \left[\Delta\Lambda_0^2 + 0.33\,(1-\Lambda_0)\ln\left(\upsilon^3 + \frac{\upsilon_{\rm c}^3}{\upsilon^3(1+\upsilon_{\rm c}^3/\upsilon_0^3)}\right)\right]^{1/2}, \tag{2}$$

υ_0 is the beam ion injection speed, c is the normalized factor, υ_c is the critical velocity, $P_\phi = \psi + \upsilon_\parallel I/\Omega_h$ is the canonical momentum, $I = RB_\phi$, $\Omega_h = ZeB/m_h$, and $\langle\cdots\rangle$ denotes orbit average. $\Lambda_0 = 0.6$ is the central pitch angle, $\Delta\Lambda = 0.2$, $\Delta\psi = 0.37(\psi_{max} - \psi_{min})$. The beam ion distribution function considers the pitch angle scattering. The maximum gyroradius of energetic particle is $\rho_h = 0.085a$ for $\upsilon_h = 2.55\upsilon_A$. For simplicity, the energetic particle collision with thermal ions and electrons are not considered in the model, and the source and sink for energetic particles are also not included in the simulations.

3. Simulation results

3.1. Nonlinear evolution of the single-n TAE mode

We first study the nonlinear evolution of the TAE mode with single-n ($n_{single} = 1$ or 2) as a reference case. Figure 1 shows the time evolution of the TAE mode kinetic energy (a) and frequency [(b), (c)]. The mode frequency chirping is due to the evolution of the phase space structure. The injection speed range of beam ions $\upsilon_h = [2.19, 3.29]\,\upsilon_A$ is used in the $n_{single} = 1$ case. Figure 2 shows the locations of the single-n TAE modes.

Figure 3 shows the single-n ($n_{single} = 1$, 2) TAE mode structure at three different times: [(a), (d)] in the linear phase, [(b), (e)] in the initial saturation phase, and [(c), (f)] in the late saturation phase. Here U is the velocity stream function of the incompressible part of the perturbed plasma velocity. TAE is characterized with two dominant poloidal harmonics (m and $m+1$) localized between two mode rational surfaces. It is observed that for the $n_{single} = 1$ mode, the structure with the dominant $m/n = 1/1$ component in the initial saturation phase is similar to that in the linear phase.

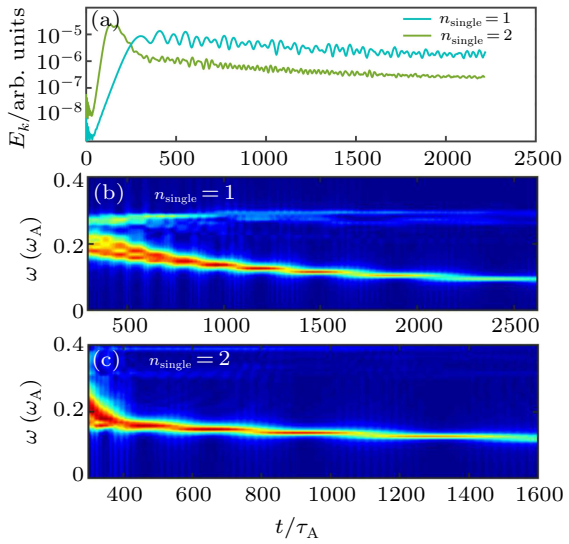

Fig. 1. Nonlinear evolution of TAE mode: (a) time evolution of single-n ($n_{single} = 1, 2$) TAE mode kinetic energy, (b) and (c) fourier spectrogram of single-n ($n_{single} = 1, 2$) TAE mode.

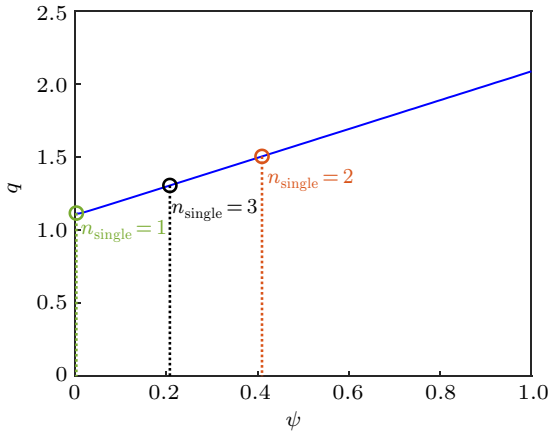

Fig. 2. The safety factor equilibrium profile and the locations of the single-n ($n_{single} = 1, 2, 3$) TAE modes.

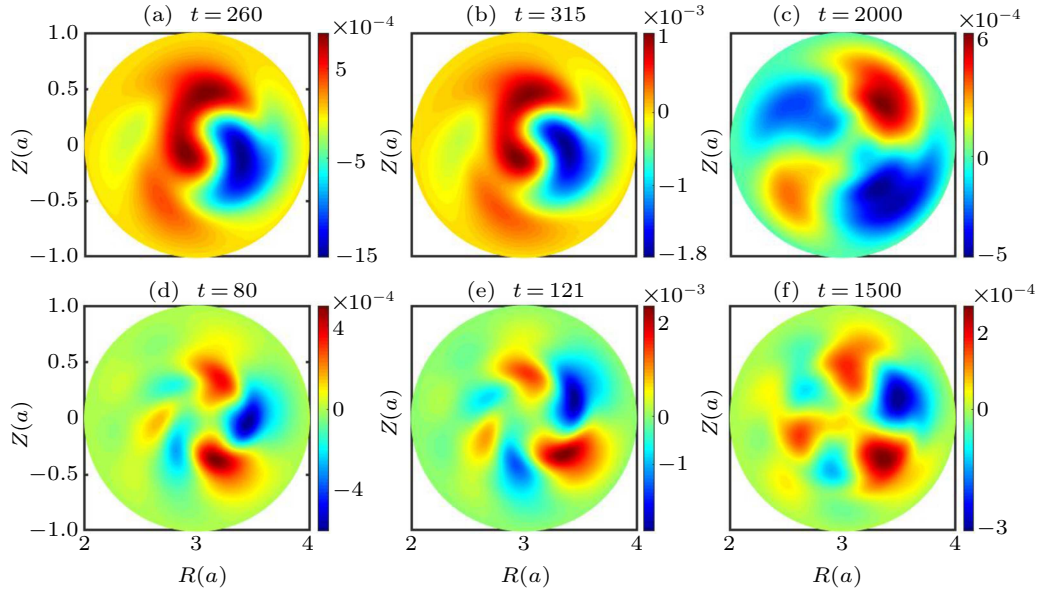

Fig. 3. The single-n ($n_{single} = 1, 2$) TAE mode structure of velocity stream function (U) at three time slices: [(a), (d)] in the linear phase, [(b), (e)] in near initial saturation, [(c), (f)] in late nonlinear phase.

In the late saturation phase of the evolution, however, the mode structure changes significantly with the dominant $m/n = 2/1$ component, as shown in Figs. 3(a)–3(c). It coincides with the fact that the $n_{\rm single} = 1$ mode we investigate here produces the pitch-fork phenomenon and has two branches: down-chirping branch and up-chirping branch, as shown in Fig. 1(b). It is known that frequency chirping is always accompanied by the redistribution of energetic ions. The gradient of energetic ions near the resonant surface $q = 1.5$ may change. Thus the dominate mode is changed from $m = 1$ to $m = 2$. However, for the $n_{\rm single} = 2$ case, the $m/n = 3/2$ mode is always dominant. This is due to the fact that the $n_{\rm single} = 2$ mode has only one branch, i.e., down-chirping branch, as shown in Fig. 1(c).

It is known that the fast ions can destabilize Alfvén waves by passing and/or trapped particle resonance via tapping the free energy associated with fast ion pressure nonuniformity. The TAE modes can be excited by the free energy associated with fast ion pressure gradient through wave particle resonant interaction due to the fact that they are discrete in nature and have weak continuum damping. The wave particle resonant interaction mathematically can be described as the resonant condition $n\omega_{\rm t} + p\omega_{\rm p} - \omega = 0$, where p is an integer, ω is the mode frequency, $\omega_{\rm t} = \Delta\phi/\Delta t$, $\omega_{\rm p} = 2\pi/\Delta t$ are both bounce-average frequency in the calculation and Δt is the time for each particle to complete one round poloidally. For passing particles, $\omega_{\rm t}$ is toroidal transit frequency and $\omega_{\rm p}$ is poloidal transit frequency. For trapped particles, $\omega_{\rm t} \equiv \omega_{\rm d}$ is toroidal precession drift frequency and $\omega_{\rm p}$ is poloidal bounce frequency. If the right wave-particle phase is given, the linear momentum exchange may cause convective loss of fast ions. However, when the trajectories of resonant fast ions overlap with mode spatial structure, the fast ion stochastic diffusion is induced, thus a global redistribution of fast ions may occur. In Fig. 4, the beam ion perturbation distribution function δf for $n_{\rm single} = 1$ is plotted, and the resonant particle locations in P_ϕ–E phase space around $\mu = 5.225$ (normalized by E_0/B_0) are traced. The selected value of magnetic moment μ is a typical one, which contains the most regions of both passing and trapped resonant particles, around which the perturbation distribution function δf is relatively larger. Multiple kinds of fast ions and resonances exist in the system since the TAE instability in this work is studied with a beam ion distribution function including the beam ion pitch angle scattering effect. It is shown in Fig. 4 that the primary resonances are $p = 1$ and $p = 2$ for trapped particles, $p = 1$ for co-passing particles, and $p = 2$ for counter-passing particles.

For the single-n case, the moment of a particle in phase space can be described mathematically as

$$\frac{{\rm d}P_\phi}{{\rm d}t} = -\frac{n}{\omega}\frac{{\rm d}E}{{\rm d}t}. \tag{3}$$

In axisymmetric time-independent fields, energy E and toroidal angular momentum P_ϕ are conserved along the particle orbit. In the presence of a wave with angular frequency ω and toroidal mode number n, neither energy nor toroidal momentum is conserved. However, a combination of energy and toroidal momentum $E' = E - \omega P_\phi/n$ is a conserved.[32] Accordingly, equation (3) can be obtained. Equation (3) means that the change of particle toroidal angular momentum is proportional to the change of particle energy in the presence of a perturbation with the frequency ω and toroidal mode number n. Since P_ϕ can be considered as a radial variable, this means that a particle moves outside radially with decreasing energy or moves inside radially with increasing energy.

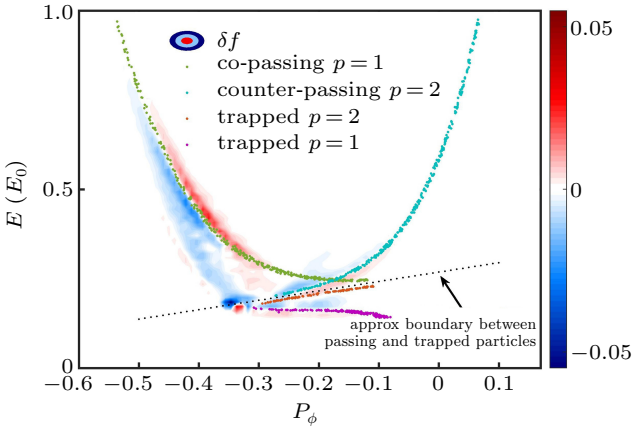

Fig. 4. For $n_{\rm single} = 1$ the perturbed distribution function δf around the magnetic moment $\mu = 5.225$ in phase space of canonical momentum and energy, i.e., P_ϕ–E. For a fixed E, small P_ϕ corresponds to the plasma core and large P_ϕ corresponds to the plasma edge.

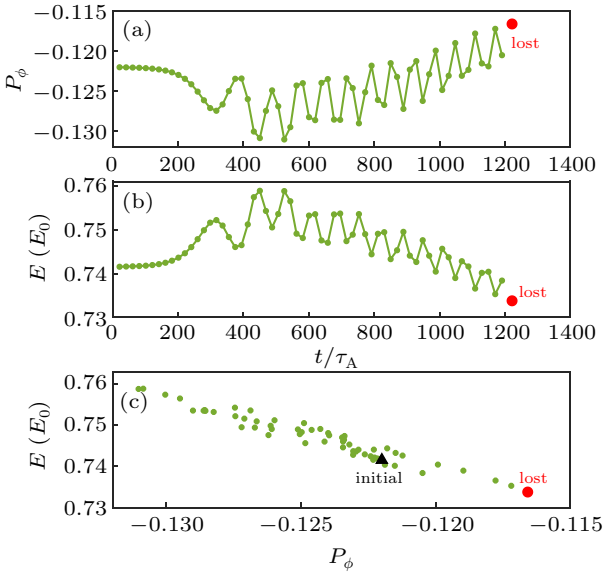

Fig. 5. The evolution of P_ϕ (a), E (b) and the trajectory (c) of a typical initially resonant particle in the $n_{\rm single} = 1$ simulation. Note that the red dot "lost" in the figure denotes the position at the lost moment and that the black triangle "initial" in subplot (c) denotes the position at initial moment.

To analyze the loss mechanism in the $n_{\rm single} = 1$ case, a typical lost particle is taken to represent the lost particle resonant with the $n_{\rm single} = 1$ mode. Figures 5(a) and 5(b) show

the time evolution of P_ϕ and energy E, respectively, and Figure 5(c) shows the position of the lost particle in the P_ϕ–E phase space. P_ϕ can be regarded as a radial variable, and the change of P_ϕ can represent the size and motion of saturated island, since P_ϕ conservation is broken in the presence of the perturbation. The mode's growth and chirping induce island broadening and drift. When the saturated island moves outwards and intersects with the loss boundary, the fast ion may pass the last closed flux surface. It is found from Fig. 5 that with the TAE mode growth (see Fig. 1(a)), the saturated island becomes broad, first moves inwards radially and then outwards.

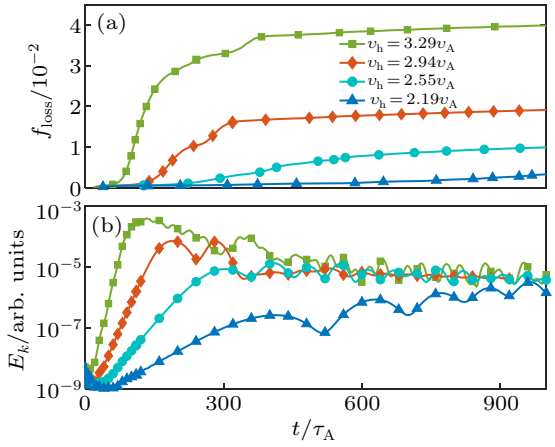

Fig. 6. (a) The time evolution of the loss level $f_{\rm loss}$ and (b) the time evolution of the mode energy in the $n_{\rm single}=1$ case for $\upsilon_{\rm h}=[2.19,3.29]\,\upsilon_{\rm A}$ with the fast ion beta $\beta_{\rm h}=1.81\%$.

To study the effect of the beam ion injection speed on the beam ion loss, the time evolution of the beam ion loss induced by the $n_{\rm single}=1$ TAE mode is given in Fig. 6. Here $f_{\rm loss}$, representing the beam ion loss level, is defined as

$$f_{\rm loss}(t)=\frac{n_{\rm loss}(t)}{n(0)}, \tag{4}$$

where $n_{\rm loss}(t)$ is the overall amount of lost particles at time t (running outside of the plasma during the evolution of the TAE mode), $n(0)$ is the total loaded particles. It is clearly shown in Fig. 6(a) that the overall loss level increases with the beam ion injection speed. This is mainly due to the fact that the large beam ion injection speed leads to a long slowing-down time and a high energy gained from the resonant beam ions. On the other hand, the larger beam ion injection speed results in a larger orbit width, leading to the higher level anomalous transport and higher level beam ion losses. Moreover, it is seen in Fig. 6(b) that the linear growth rate and nonlinear amplitude also increase with the injection speed. Since no particle source is available in the simulation model and the saturated mode amplitude is relatively low (10^{-5}) in the late nonlinear phase, the beam ion loss mainly appears in the linear and early nonlinear phase but become very weak the later nonlinear phase, at least for the parameters studied here.

3.2. Interaction between modes and resonance overlap in multiple-n simulation

In this section, the results of simulations simultaneously including n (or $n_{\rm multiple}$) = 1–4 modes (multiple-n case) are presented. The parameters used in the multiple-n simulation are the same as those in the $n_{\rm single}=1$ simulation (see Section 2). Comparisons are also made with the results of simulations including only one individual mode (single-n cases). The evolutions of the $n=1$, $n=2$, $n=3$, and $n=4$ mode amplitudes in multiple-n and single-n simulations are compared in Fig. 7. In the multiple-n simulation, the $n>4$ fluctuations are filtered out, so only $n=1$, $n=2$, $n=3$, $n=4$ modes are kept. It is clearly observed that due to the nonlinear interaction between different n modes, the evolution of $n=1$ mode is significantly different after $t/\tau_{\rm A}\geqslant 300$. The $n=1$ mode amplitude in the multiple-n simulation is clearly reduced by such nonlinear interactions after $t/\tau_{\rm A}\geqslant 300$. Moreover, the $n=4$ mode in the single-n case is stable, while it is unstable in the multiple-n case. The mode frequency evolution of $n=1$, $n=2$, $n=3$, $n=4$ modes are shown in Fig. 8. Since two possible free energy channels, wave-wave coupling and wave-particle interaction, exist for Alfvén wave instabilities, there are two possible explanations for the $n=4$ mode excitation. However, we have examined the frequency matching condition between $n=4$ and $n=2$, between $n=4$ and $n=13$, and it is found that the frequency matching condition is not satisfied very well. One possible mechanism for $n=4$ mode excitation is due to the wave-particle interaction. Since the redistribution and loss of energetic ions induced by $n=1$, $n=2$, $n=3$ modes lead to the modification of energetic ion density gradient, the $n=4$ mode can be excited.

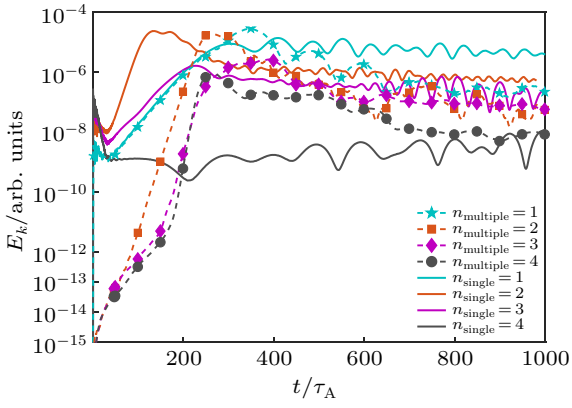

Fig. 7. Nonlinear evolution of kinetic energy E_k for multiple-n and single-n cases with $\beta_{\rm h}=1.81\%$ and beam ion injection speed $\upsilon_{\rm h}=2.55\upsilon_{\rm A}$. Multiple-$n$ ($n_{\rm multiple}=1,2,3,4$) stands for $n=1,2,3,4$ in the multiple-n cases, respectively. Single-n ($n_{\rm single}=1,2,3,4$) stands for $n=1,2,3,4$ in the single-n cases, respectively. The growth rates of $n_{\rm multiple}=1,2,3,4$ modes are $\gamma_{n=1}=0.0167\omega_{\rm A}$, $\gamma_{n=2}=0.0525\omega_{\rm A}$, $\gamma_{n=3}=0.0656\omega_{\rm A}$, $\gamma_{n=4}=0.0937\omega_{\rm A}$, respectively.

In general, multiple modes can interact with each other indirectly via mutual scattering effect on their individual resonant particles. Such indirect interaction may occur in two

ways. On the one hand, the modes have to share the energy delivered by the particles. On the other hand, the energy can also be transferred when a particle is scattered from one mode into the other mode instead of escaping from the wave. Such a particle recycling, as well as multiple resonances covering a large region of phase space, can also increase the total energy transferred to the fluctuating fields in the multiple-n simulation. This can be easily seen in Fig. 7 by comparing the mode energies between the single-n and multiple-n cases.

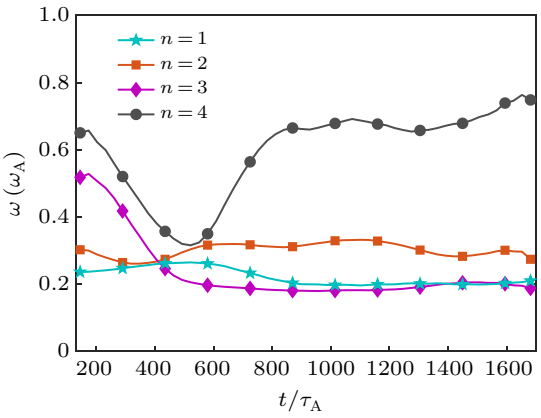

Fig. 8. The mode frequency evolutions of $n=1$, $n=2$, $n=3$, $n=4$ modes with the observation of mode frequencies chirping down or up in the multiple-n simulation.

Moreover, the wave-particle resonance and particle trajectory in the phase space are analyzed. The orbits of beam ions are usually defined by three invariants of the motions: the energy E, the magnetic moment μ, and the toroidal canonical momentum P_ϕ. When a resonant interaction between a mode and a beam ion takes place, the magnetic moment μ of the ion is conserved, whereas both the energy E and the toroidal canonical momentum P_ϕ change during the process. In Fig. 9, the particle trajectories in P_ϕ–E space are followed in the presence of time-dependent multiple-n TAE perturbation, and the position in P_ϕ–E phase space is recorded when each particle passes through the mid-plane. The different components of the multiple-n mode are represented by different colors: $n=1$ (red), $n=2$ (green), $n=3$ (black), $n=4$ (blue). The initially resonant particles are with a fixed value of magnetic moment $\mu=9.933$ (normalized by E_0/B_0). Of particular concern in the multiple-n case is whether the mode amplitudes become large enough to cause resonances overlap, which can determine the global fast ion loss. It is found that the resonance overlap is greatly facilitated by the simultaneous excitation of multiple modes, as studied previously.[33] Moreover, when the closely spaced resonances overlap, there is an enhanced release of mode energy, which in turn can cause nearby but more widely spaced resonances to overlap. This thereby rapidly expands the phase space region over which particles are redistributed to the plasma edge or lost. Figure 10 indicates that the radial mode structures overlap in the radial direction, in particular for the $n_{\rm multiple}=1,2$ modes in the multiple-n case. As a result, the resonances in the P_ϕ–E phase space are neighboring and thus easily overlap for the multiple-n case, especially at higher amplitudes. This resonance overlap in the phase space is evidently observed for the multiple-n case in Fig. 9(a). Although the modes discussed here come from the components of multiple-n TAE, one can clearly see the overlap, especially in the region of the low energetic particles.

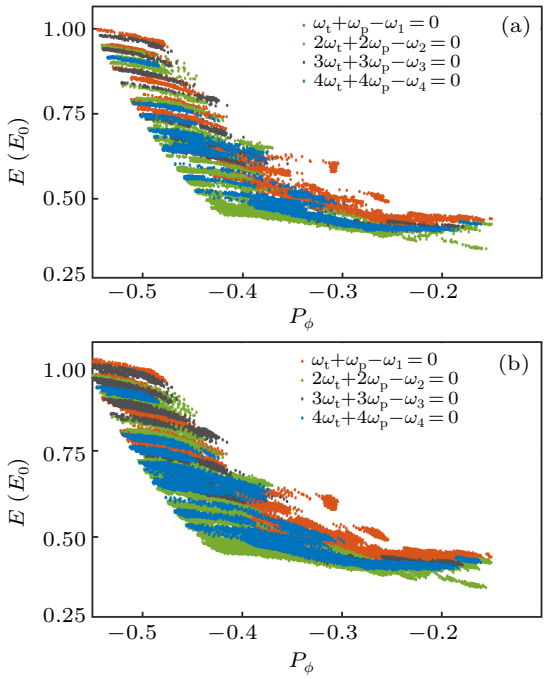

Fig. 9. The weak resonance-overlapping multiple-n TAE ($\beta_h=1.81\%$) (a) and the relatively strong resonance-overlapping multiple-n TAE ($\beta_h=6\%$) (b). Fast ion trajectories in the phase space of canonical momentum P_ϕ and energy E in the presence of multiple-n TAE modes at $t=0$–$2000\tau_A$. Only the initially resonant particles are plotted in the figure. The particles which initially resonate with the different components of the multiple-n mode are represented by colors: $n=1$ (red), $n=2$ (green), $n=3$ (black), $n=4$ (blue). Since the particles are trapped by the $n=1,2,3,4$ modes, the positions of resonant particles in phase space can be regarded as the eigenmodes. Namely, the eigenmodes are represented by colors: $n=1$ (red), $n=2$ (green), $n=3$ (black), $n=4$ (blue). The frequencies of $\omega_1,\omega_2,\omega_3,\omega_4$ stand for the mode frequencies of $n=1,2,3,4$, respectively, in the multiple-n case.

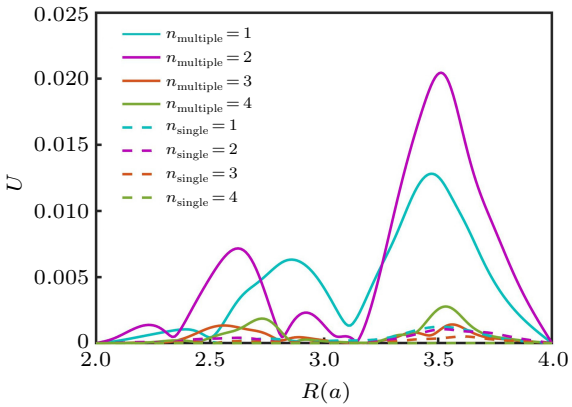

Fig. 10. Comparison of velocity stream function at the midplane with $t=251\tau_A$ in the multiple-n ($n_{\rm multiple}=1,2,3,4$) and single-n ($n_{\rm single}=1,2,3,4$) simulations.

Note that although a particle can be lost in the $n_{\rm single}=1$ or 2 mode, or other TAE mode, it is only recorded as one lost particle in the sum loss of all individual single-n modes. That is, this sum loss is not the simple addition of all individual single-n losses. Therefore, it is shown in Fig. 11 and Table 1 that in the single-n case, the sum loss level is certainly higher than the loss level from any single-n mode, though less than the loss level from the simple addition of all individual single-n losses. Even more important, it is interestingly found that the loss level in the multiple-n case is rather higher than the sum loss level in the single-n case because of the resonance overlap. Such a loss level increase in the multiple-n case is enhanced by 16% for $\beta_{\rm h}=1.81\%$. Further simulations indicate that increasing $\beta_{\rm h}$ can significantly rise the loss level in the multiple-n case.

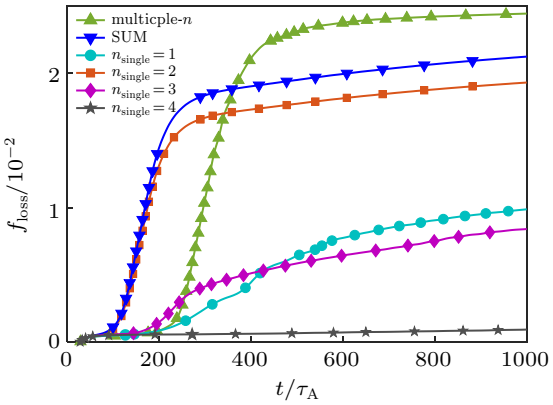

Fig. 11. Evolutions of the level of beam ion losses $f_{\rm loss}$ in $n_{\rm single}=1$, $n_{\rm single}=2$, $n_{\rm single}=3$, $n_{\rm single}=4$ simulations and multiple-n simulation with the same parameter $\beta_{\rm h}=1.81\%$, $\upsilon_{\rm h}=2.55\upsilon_{\rm A}$. Note that sum denotes the sum of loss over $n_{\rm single}=1$–4 modes, where every lost particle is calculated for one time.

Table 1. Comparison of the linear growth rate and fast ion losses in the single-n and multiple-n cases. Note that every lost particle is calculated for one time.

Simulation type	Growth rate	Loss fraction/%
multiple-n TAE	for $n_{\rm multiple}=1,2,3,4$ 0.0167, 0.0525, 0.0656, 0.0937	2.45
$n_{\rm single}=1$ TAE	0.0167	0.98
$n_{\rm single}=2$ TAE	0.0511	1.93
$n_{\rm single}=3$ TAE	0.0178	0.84
$n_{\rm single}=4$ TAE	stable	0.09
Sum		2.12

Figure 12 shows that for $\beta_{\rm h}=6.0\%$, the loss level is greatly enhanced and even reaches $\sim 13\%$ of beam ions, approximately 5 times higher than that for $\beta_{\rm h}=1.81\%$. This significant increment may result from the strong resonance overlap, as shown in Fig. 9(b). Once the overlap of closely spaced resonances occurs in the multiple-n case, the release of mode energy is increased so that the widely spaced resonances can also take place. As a result, such a process can effectively enlarge the phase space region and then particles are redistributed or lost. It is also demonstrated that the trajectory of the same lost ions in the presence of the multiple-n TAE is significantly different from that in the presence of the single-n TAE. Additionally, the loss level increment between the multiple-n and single-n cases is enhanced to 44% for $\beta_{\rm h}=6.0\%$. This high loss level is indeed of critical importance for the fast ion confinement in high parameter plasmas like in ITER and CFETR.

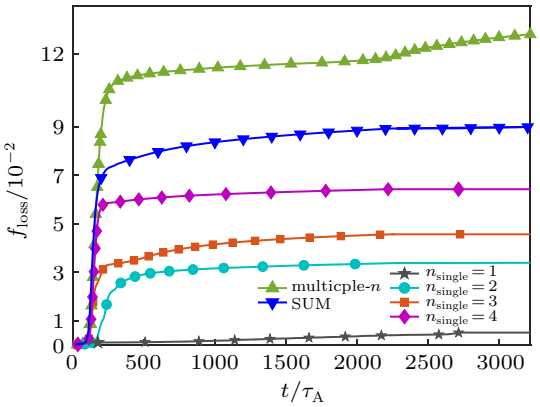

Fig. 12. Evolutions of the level of beam ion losses $f_{\rm loss}$ in $n_{\rm single}=1$, $n_{\rm single}=2$, $n_{\rm single}=3$, $n_{\rm single}=4$ simulations and multiple-n simulation with high fast ion beat $\beta_{\rm h}=6\%$, $\upsilon_{\rm h}=2.55\upsilon_{\rm A}$. Every lost particle is calculated for one time.

The evolution of P_ϕ is given in Fig. 13(a), which can be regarded as a radial variable used to describe the radial position of a particle. The particle we plot here is a typical resonant trapped particle which is initially in resonance with the multiple-n TAE mode. The oscillation of P_ϕ shown by the green triangles indicates that the particle is trapped in the multiple-n TAE mode. In comparison with the single-n cases, the amplitude of oscillation of P_ϕ in the multiple-n simulation is much larger, especially in the later nonlinear phase. Figure 13(b) indicates that the energy change in the multiple-n simulation (shown by green triangles) is significantly larger than that in the single-n simulation. This is due to the fact that the particles can have multiple resonances and the overlap even occurs in the multiple-n simulation, increasing the total energy transferred to the background plasmas. For the $n_{\rm single}=1$ case, the oscillation of P_ϕ indicates that the particle is also trapped by the mode. At each resonance, the wave-particle momentum exchange, proportional to the mode perturbation amplitude, corresponds to a radial drift. It is found by comparison that in spite of the same particles in the simulations, the trajectories and the energy changes in the presence of different n modes are quite different from each other. For example, the trajectories of the particle studied here in the multiple-n and $n_{\rm single}=1$ simulations all exhibit diffusive characteristic, since such random walk (oscillation of P_ϕ) is the typical character of diffusive fast ion transport. However, in the $n_{\rm single}=2$ and 3 simulations, a convective characteristic

is exhibited since direct walk is the typical character of convective fast ion transport. Finally, according to Eq. (3) and the change of P_ϕ, it is revealed that the particles in the $n_{\rm single}=1$ and 3 simulations gain energy, while those in the multiple-n and $n_{\rm single}=2$ simulations lose energy.

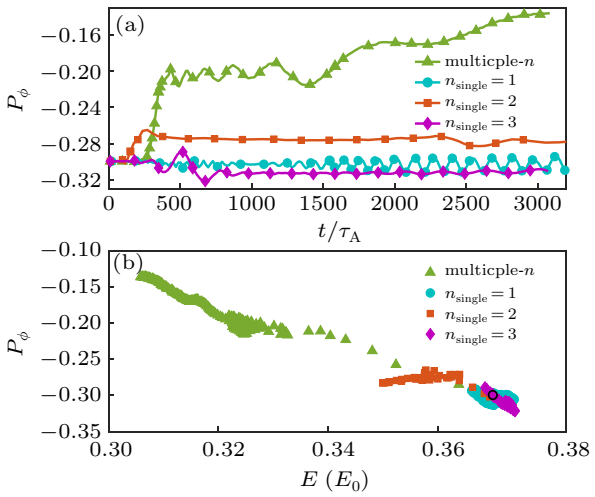

Fig. 13. Comparison of the evolution of P_ϕ (a) and the trajectory (b) of a typical initially resonant particle in multiple-n simulation with that in the $n_{\rm single}=1$, $n_{\rm single}=2$ and $n_{\rm single}=3$ simulations. The black circle denotes initial position of the particle in phase space.

3.3. Phase-space characterization of losses in the single-n and multiple-n simulations

Figure 14 gives the distributions of lost beam ions in the phase space of the beam ion energy E and the change of pitch angle $\Delta\Lambda$ in the single-n and multiple-n simulations. It should be noted that the loss discussed here is all associated with the presence of TAE. As observed in Fig. 14, a slight shift of the beam ion losses is towards the higher pitch angle Λ value in the single-n and multiple-n simulations. Aside from the dominant characteristic, there are some other lost beam ions for which the pitch angles become lower. Since the definition of pitch angle Λ in the M3D-K code depends on the energy (see Section 2), it is changed to

$$\Delta\Lambda=-\frac{\mu B_0\left(E_{\rm f}-E_{\rm i}\right)}{E_{\rm i}E_{\rm f}}=-\frac{\mu B_0\Delta E}{E_{\rm i}E_{\rm f}}, \tag{5}$$

where $E_{\rm i}$ and $E_{\rm f}$ are the initial and the final energies of beam ion, respectively, and ΔE is the change of energy. Thus, we can conclude that most of the lost particles contribute energy to the TAE mode while very few parts of lost particles gain energy from the TAE mode.

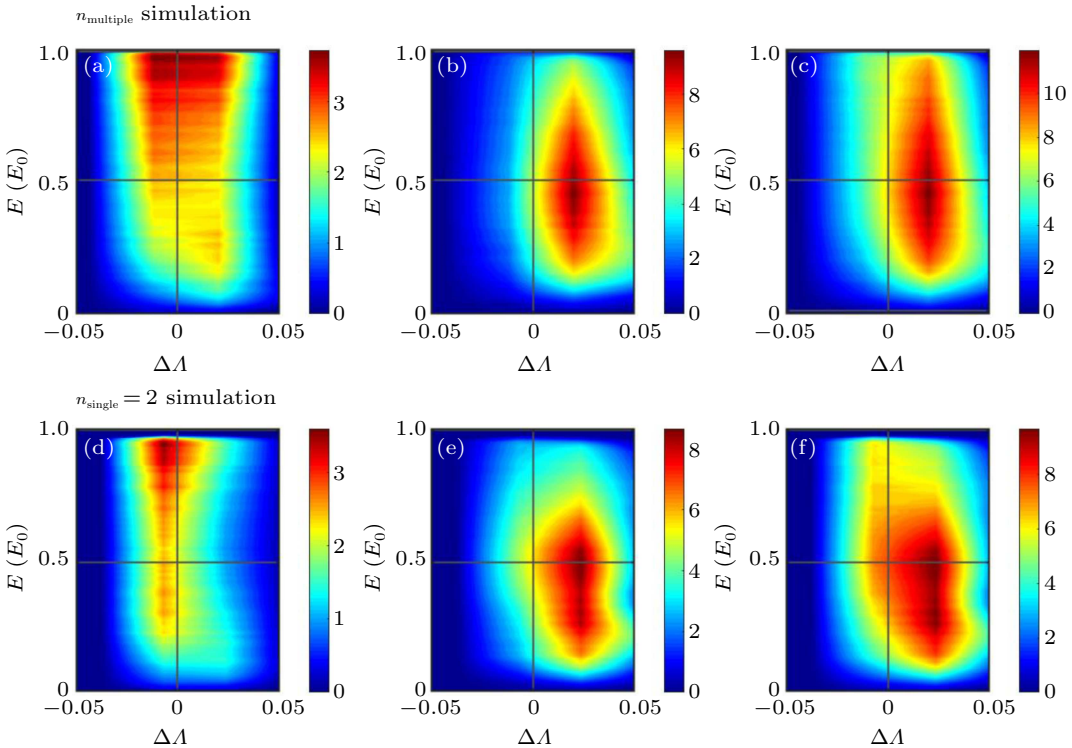

Fig. 14. Comparison of distribution of lost beam ions in E–$\Delta\Lambda$ space for (a)–(c) multiple-n and (d)–(f)$n_{\rm single}=2$ simulations with the same parameter $\beta_{\rm h}=1.81\%$, $\upsilon_{\rm h}=2.55\upsilon_{\rm A}$, where E is referred to the energy of lost beam ion at the lost moment and $\Delta\Lambda$ is referred to the difference between the pitch angle Λ_{l1} at the lost moment and the pitch angle Λ_{l0} at the initial moment when the particle has not suffered from the perturbation. [(a), (d)] The lost passing particle distribution in each simulation. [(b), (e)] The lost trapped particle distribution in each simulation. [(c), (f)] The overall lost particle distribution in each simulation. The color coding is in arbitrary units.

Table 2 gives a summary of the loss fraction characterized by contributing energy to the wave and the loss fraction of trapped ions in the single-n and multiple-n simulations. It is found that in both the single-n and multiple-n simulations, the main loss mechanism is through contributing energy to the wave. This is due to the fact that when a beam ion drives the

mode, its energy decreases ($\Delta E < 0$) and then it moves radially outward in the minor radius ($\Delta P_\phi > 0$) and eventually may be easily lost. However, a small fraction ($\sim$5%) of the fast ion losses characterized by gaining energy from wave is observed in both the single-n and multiple-n simulations. This may be due to the fact that the particle is accelerated and its orbit is influenced.[34]

Table 2. A statistical analysis on the characteristics of fast ion losses performed. The contributing energy is a ratio of the amount of losses that contribute energy from wave to the total amount of losses. The trapped fraction is a ratio of the number of lost trapped particles to the total number of lost particles.

Simulation type	Contributing energy/%	Trapped fraction/%
multiple-n TAE	93	72
$n_{\text{single}} = 1$ TAE	95.48	78.93
$n_{\text{single}} = 2$ TAE	95.16	76.82
$n_{\text{single}} = 3$ TAE	96.90	81.60

Another characteristic in common, as shown in Table 2, is that the lost fraction of trapped ions is two to four times larger than that of passing ions. Particles traveling on banana orbits are more easily lost, since the trapped orbits are wider. Especially for so-called 'potato orbits', they are more sensitive to the perturbation near their turning points. For passing particles, in addition, the transformation from passing particles to trapped particles during the nonlinear evolution of TAE mode is a well-known loss mechanism for beam ions. Also, we can find that the multiple-n simulation has a higher fraction of lost fast ions coming from passing population. It can be attributed to the fact that compared with the single-n case, more passing particles can gain energy from the multiple-n TAE modes and render their orbits to become unconfined.

4. Discussion and summary

In summary, nonlinear evolution of multiple TAEs driven by fast ions is self-consistently investigated using kinetic simulations with the M3D-K code. A beam ion distribution function is considered, in which the pitch angle scattering is included. Some typical characteristics of single-n ($n = 1, 2$) TAE, for example, mode frequency chirping and the dynamics of resonant excitation, are obtained. Meanwhile, the increasing tendency for overall loss level with increasing beam ion injection speed is observed. This is mainly due to the fact that the large beam ion injection speed leads to a long slowing-down time and a high energy gained from the resonant beam ions. On the other hand, the larger bean ion injection speed results in a larger orbit width, leading to the higher level anomalous transport and higher level beam ion losses. In the self-consistent simulation, the mode's growth and chirping induce island broadening and drift, which is the main reason of single-n TAE mode induced ion losses.

Even more importantly, it is interestingly found that in the multiple-n case, the fast ion loss level is rather higher than the sum loss level from all individual single-n modes in the single-n case. Moreover, increasing fast ion beta β_{h} can not only significantly increase the loss level in the multiple-n case but also significantly increase the loss level increment between the single-n and multiple-n cases. For example, the loss level in the multiple-n case for $\beta_{\text{h}} = 6.0\%$ can even reach 13% of the beam ions and is 44% higher than the sum loss level calculated from all individual single-n modes in the single-n case. The high loss level is indeed of critical importance for the fast ion confinement in high parameter plasmas like in ITER and CFETR. This significant increment may result from the strong resonance overlap. Once the closely spaced resonance overlap occurs in the multiple-n case, the release of mode energy is increased so that the widely spaced resonances can also take place. As a result, such a process can effectively enlarge the phase space region and then particles are redistributed or lost. It is also demonstrated that the trajectory of the same lost ions in the presence of multiple-n TAE is significantly different from that in the presence of single-n TAE.

On the other hand, a slight shift of the beam ion losses is towards the higher pitch angle Λ value in the single-n and multiple-n simulations. The main loss mechanism is through contributing energy to the wave, which is due to the fact that when a beam ion drives the mode, its energy decreases ($\Delta E < 0$) and then it moves radially outward in the minor radius ($\Delta P_\phi > 0$) and eventually may be easily lost. The lost fraction of trapped particles is 2–4 times larger than that of passing particles. Particles traveling on banana orbits are more easily lost since the trapped orbits are wider. Especially for so-called 'potato orbits', they are more sensitive to the perturbation near their turning points.

In fact, fast ion loss is a very complicated issue, because it can be influenced by many elements such as the mode structure, the selected configuration, and the employed parameters. Usually, only one mechanism cannot account for the complicated physical process. Likewise, several kinds of fast ion loss mechanisms, such as prompt loss, mode-particle pumping and non-resonant loss mentioned in the introduction, coexist in our simulation. Prompt losses are the ones of particles born on perturbed orbits that collide with the first wall. In our simulation, a certain fraction of fast ions, passing through the plasma domain after several bounce periods, is prompt losses. The non-resonant losses are the ones of particles without resonance with the mode. Usually, some fraction of fast ions must become lost particles in the NBI-born fast ion simulation, regardless of the presence of the perturbation or not. The mode-particle pumping is actually a resonant phenomenon, where the loss results from the wave-particle resonance. This loss mechanism is also present because the TAE mode is mainly excited by the wave-particle resonance in our model. Therefore, fast ion loss is actually a very complicated important

problem, and these several kinds of loss mechanisms mentioned above coexist in our simulation.

A major effort spent in the present work is aimed at understanding the general characteristic of beam ion loss in the presence of the single-n and multiple-n TAEs. It is also interesting to investigate and assess the beam ion loss in the coexistence of multiple kinds of instabilities, such as fishbone modes and TAEs under the realistic profiles observed experimentally or the predicted profiles on the CFETR. A hybrid gyro-kinetic linear simulation by Chen *et al.*[35] indicated that the most unstable modes in reactor, such as the ITER, lie in the range of $10 < n < 20$. The physics of $10 < n < 20$ Alfvén eigenmodes is significantly crucial for future reactor. Global nonlinear simulations of beam ion loss considering beam ion source and sink are also important to be studied. We leave these subjects to the future works.

Acknowledgments

We gratefully thank Professor G. Y. Fu, and Dr. J. Zhu for some valuable suggestions and discussions. The authors acknowledge the Supercomputer Center of Dalian University of Technology for providing computing resources.

References

[1] Chen L 2008 *Plasma Phys. Control. Fusion* **50** 124001
[2] Chen L and Zonca F 2016 *Rev. Mod. Phys.* **88** 015008
[3] Todo Y 2019 *Rev. Mod. Plasma Phys.* **3** 1
[4] Aymar R, Chuyanov V A, Huguet M, Shimomura Y, ITER Joint Central Team and ITER Home Teams 2001 *Nucl. Fusion* **41** 1301
[5] Wan Y X, Li J G, Liu Y, Wang X L, Chan V, Chen C A, Duan X R, Fu P, Gao X, Feng K M, Liu S L, Song Y T, Wen P D, Wan B N, Wan F R, Wang H Y, Wu S T, Ye M Y, Yang Q W, Zheng G Y, Zhuang G, Li Q and Team CFETR 2017 *Nucl. Fusion* **57** 102009
[6] Fasoli A, Gormenzano C, Brek H L, Breizman B, Briguglio S, Darrow D S, Gorelenkov N, Heidbrink W W, Jaun A, Konovalov S V, Nazikian R, Noterdaeme J M, Sharapov S, Shinohara K, Testa D, Tobita K, Todo Y, Vlad G and Zonca F 2007 *Nucl. Fusion* **47** S264
[7] Garcia-Munoz M, Hicks N, Van-Voomveld R, Classen I G J, Bilato R, Bobkov V, Bruedgam M, Fahrbach H U, Igochine V, Jaemsae S, Maraschek M, Sassenberg K and ASDEX Upgrade Team 2010 *Phys. Rev. Lett.* **104** 185002
[8] Podesta M, Heidbrink W W, Liu D, Ruskov E, Bell R E, Darrow D S, Fredrickson E D, Gorelenkov N N, Kramer G J, LeBlanc B P, Medley S S, Roquemore A L, Crocker N A, Kubota S and Yuh H 2009 *Phys. Plasmas* **16** 056104
[9] Nabais F, Kiptily V G, Pinches S D, Sharapov S E and contributors A 2010 *Nucl. Fusion* **50** 084021
[10] Duong H H, Heidbrink W W, Strait E J, Petrie T W, Lee R, Moyer R A and Watkins J G 1993 *Nucl. Fusion* **33** 749
[11] Collins C S, Heidbrink W W, Austin M E, Kramer G J, Pace D C, Petty C C, Stagner L, Van Zeeland M A, White R B, Zhu Y B and team DIII-D 2016 *Phys. Rev. Lett.* **116** 095001
[12] Heidbrink W W, Collins C S, Podesta M, Kramer G J, Pace D C, Petty C C, Stagner L, Van Zeeland M A, White R B and Zhu Y B 2017 *Phys. Plasmas* **24** 056109
[13] Bass E M and Waltz R E 2017 *Phys. Plasmas* **24** 122302
[14] Schneller M, Lauber Ph and Briguglio S 2016 *Plasma Phys. Control. Fusion* **58** 014019
[15] Chen L and Zonca F 2007 *Nucl. Fusion* **47** S727
[16] Chen X, Heidbrink W W, Kramer G J, Van-Zeeland M A, Austin M E, Fisher R K, Nazikian R, Pace D C and Petty C C 2013 *Nucl. Fusion* **53** 123019
[17] White R B, Goldston R J, McGuire K, Boozer A H, Monticello D A and Park W 1983 *Phys. Fluids* **26** 2958
[18] Tobita K, Tani K, Nishitani T, Nagashima K and Kusama Y 1994 *Nucl. Fusion* **34** 1097
[19] Zhang R B, Fu G Y, White R B and Wang X G 2015 *Nucl. Fusion* **55** 122002
[20] Park W, Belova E V, Fu G Y, Tang X Z, Strauss H R and Sugiyama L E 1999 *Phys. Plasmas* **6** 1796
[21] Fu G Y, Park W, Strauss H R, Breslau J, Chen J, Jardin S and Sugiyama L E 2006 *Phys. Plasmas* **13** 052517
[22] Wang F, Fu G Y, Breslau J A, Tritz K and Liu J Y 2013 *Phys. Plasmas* **20** 072506
[23] Wang F, Fu G Y, Breslau J A and Liu J Y 2013 *Phys. Plasmas* **20** 102506
[24] Wang F, Fu G Y and Shen W 2017 *Nucl. Fusion* **57** 016034
[25] Shen W, Wang F, Fu G Y, Xu L Q, Li G Q and Liu C Y 2017 *Nucl. Fusion* **57** 116035
[26] Yang S X, Hao G Z, Liu Y Q, Wang Z X, Hu Y J, Zhu J X, He H D and Wang A K 2018 *Nucl. Fusion* **58** 046016
[27] Liu D, Fu G Y, Crocker N A, Podesta M, Breslau J A, Fredrickson E D and Kubota S 2015 *Phys. Plasmas* **22** 042509
[28] Ren Z Z, Wang F, Fu G Y, Shen W and Wang Z X 2017 *Phys. Plasmas* **24** 052501
[29] Shen W, Fu G Y, Sheng Z M, Breslau J A and Wang F 2014 *Phys. Plasmas* **21** 092514
[30] Shen W, Fu G Y, Tobias B, Van-Zeeland M, Wang F and Sheng Z M 2015 *Phys. Plasmas* **22** 042510
[31] Cai H S and Fu G Y 2012 *Phys. Plasmas* **19** 072506
[32] Hsu C T and Sigmar D J 1992 *Phys. Fluids B* **4** 1492
[33] Berk H L, Breizman B N and Ye H C 1992 *Phys. Rev. Lett.* **68** 3563
[34] Galdon-Quiroga J, Garcia-Munoz M, McClements K G, Nocente M, Hoelzl M, Jacobsen A S, Orain F, Rivero-Rodriguez J F, Salewski M, Sanchis-Sanchez L, Suttrop W, Viezzer E, the ASDEX Upgrade Team and the Eurofusion MST1 Team 2018 *Phys. Rev. Lett.* **121** 025002
[35] Chen Y, Parker S E, Lang J and Fu G Y 2010 *Phys. Plasmas* **17** 102504